the exposure. It is a pleasure to thank Dr. R. Plano and his associates at Rutgers University for their collaboration in the early stages of this experiment. We would also like to express our appreciation to Professor J. Steinberger, Professor P. Franzini, and Professor C. Baltay for many illiminating discussions. We also would like to acknowledge the efforts of the Nevis and Rutgers scanning and measuring staffs, and the aid of Mrs. A. McDowell and Miss Sharon Liebeskind for the figure drawings. Finally, we would like to thank Miss Ann Therrien and Mrs. Edna Thornton for secretarial assistance.

PHYSICAL REVIEW VOLUME 156, NUMBER 5 25 APRIL 1967

Radiative Decay of the Muon*

E. BOGART,† E. DICAPUA,‡ P. NÉMETHY, AND A. STRELZOFF§
Columbia University, New York, New York
(Received 17 November 1966)

The radiative decay of the muon, $\mu^+ \rightarrow e^+ + \gamma + \nu_e + \bar{\nu}_\mu$, has been measured using muons from the Columbia University Nevis synchrocyclotron. The decay products e^+ and γ were observed at relative angles near 180°, using scintillation counters and two 9-in.×10-in. NaI crystals, which enabled simultaneous measurement of the positron and γ energies. The pulses from the crystals were displayed on oscilloscopes and photographed, and the measured amplitudes of these pulses were calibrated using the positron spectrum of the nonradiative decay. The two-dimensional energy spectrum for positrons and γ's was obtained for about 900 events, after subtraction of background. This spectrum and the measured rate, obtained by normalizing to the nonradiative decay, were compared with theoretical predictions for the radiative decay. The results were in good agreement with the theory, within statistics, for the case of pure V-A coupling.

I. INTRODUCTION

THE radiative decay of the muon, $\mu^+ \rightarrow e^+ + \gamma + \nu_e + \bar{\nu}_{\mu'}$, has been observed by several groups.[1–4] Kim, Kernan, and York[3] measured the γ spectrum at forward electron-γ angles, and Rey[4] measured the angular correlation and electron range distribution for backward electron-γ correlations. Both of these experiments obtained good agreement with theoretical predictions for the radiative mode.

Theoretical calculations for radiative muon decay were developed by many authors.[5–9] Behrends, Finkelstein, and Sirlin[6] calculated the probability of inner bremsstrahlung as part of the complete radiative corrections for muon decay; and, in fact, the agreement of the radiative decay experiments with theory has served to substantiate these radiative corrections. Fronsdal and Überall[9] worked out the most general dependence of the radiative decay process on the weak-interaction coupling constants, including parity-nonconserving combinations. They noted that the radiative decay spectrum depends on the same parameters (e.g., ρ) as the nonradiative decay, but that the spectrum is also slightly sensitive to two new parameters which, like the others, are simple functions of the coupling constants.

The present experiment was undertaken in order to measure the first of the parameters introduced by Fronsdal and Überall. This parameter, denoted by η,[10] occurs only in the radiative mode, and measures directly the fraction of scalar and pseudoscalar coupling entering into muon decay. A measurement of η is in fact most comparable to a determination of the electron polarization; and it is a well-known fact that measurements of the nonradiative decay spectrum alone, without the polarization, cannot determine the nature of the weak-interaction coupling in muon decay.

* Work supported in part by the U. S. Office of Naval Research under Contract No. Nonr-266(72).

† Present address: Department of Physics, University of Pennsylvania, Philadelphia, Pennsylvania.

‡ Present address: Instituto di Fisica dell'Università di Roma, Rome, Italy.

§ Present address: Department of Physics, University of Rochester, Rochester, New York.

[1] J. Ashkin, T. Fazzini, G. Fidecaro, N. H. Lipman, A. W. Merrison, and H. Paul, Nuovo Cimento **14**, 1266 (1959); R. R. Crittenden, W. D. Walker, and J. Ballam, Phys. Rev. **121**, 1823 (1961).

[2] D. Bartlett, S. Devons, and A. M. Sachs, Phys. Rev. Letters **8**, 120 (1962); S. Frankel, J. Halpern, L. Holloway, W. Wales, M. Yearian, O. Chamberlain, A. Lemonick, and F. M. Pipkin, *ibid.* **8**, 123 (1962); S. Frankel, W. Frati, J. Halpern, L. Holloway, W. Wales, and O. Chamberlain, Nuovo Cimento **27**, 894 (1963); S. Parker, H. L. Anderson, and C. Rey, Phys. Rev. **133**, B768 (1964).

[3] C. Kim, W. Kernan, and C. York, Phys. Rev. **120**, 983 (1960).

[4] C. Rey, Phys. Rev. **135**, B1215 (1964).

[5] A. Lenard, Phys. Rev. **90**, 968 (1953); T. Kinoshita and A. Sirlin, *ibid.* **107**, 593 (1957); S. G. Eckstein and R. H. Pratt, Ann. Phys. (N. Y.) **8**, 297 (1959).

[6] R. Behrends, R. Finkelstein, and A. Sirlin, Phys. Rev. **101**, 866 (1956).

[7] N. Tzoar and A. Klein, Nuovo Cimento **8**, 482 (1958).

[8] R. H. Pratt, Phys. Rev. **111**, 649 (1958).

[9] C. Fronsdal and H. Überall, Phys. Rev. **113**, 654 (1959).

[10] We have preserved the notation of Fronsdal and Überall in denoting this parameter by η. It should be emphasized that this parameter is not the same as the low-energy shape parameter for muon decay, which has also come to be denoted by η.

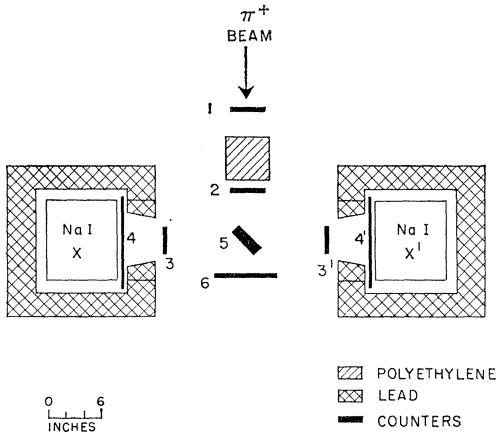

FIG. 1. Diagram of the experimental layout.

II. EXPERIMENTAL PROCEDURE

The experimental technique used was the measurement of energies of both the emitted electron and the emitted γ in the radiative decay, using two large 9-in.×10-in. NaI(Tl) crystals set at 180°. The use of the NaI crystals enabled us to obtain reasonably good energy resolution for both electron and γ. This was desirable since the theoretical spectrum for the radiative decay near 180° is in fact more sensitive to the electron and γ energies than to the electron-γ angular correlation, which could not be measured with this method. The angular region near 180° was chosen in order to obtain maximum sensitivity to the radiative decay parameter η. In addition, by looking at backwards angles, we minimized the background from electron-γ pairs following a normal bremsstrahlung, i.e., a radiation after the decay. Such events, which were indistinguishable from inner bremsstrahlung events, occur quite prolifically at forward angles, but were shown to be essentially negligible in the energy and angular region considered in this experiment.

The experimental procedure is shown in detail in Fig. 1. The beam of positive pions originated in the vibrating target of the Nevis 164-in. proton synchrocyclotron. The pions, with a mean momentum of 145 MeV/c, passed through scintillation counters 1 and 2, were slowed in $4\frac{1}{8}$ in. of polyethylene absorber, and stopped in the target counter 5. The target was 4 in.×4 in. in area, 1 in. thick, and was oriented at 45° to the incoming beam. Counter 6 was used as an anticoincidence counter, so that a stopping pion was signalled by a $125\bar{6}$ coincidence requirement. The stopping rate obtained was ~30 000 pions/sec, which was about 50% of the pions passing through beam counter 2,

The stopped pions served as a source of muons, which decayed in the radiative mode into electrons, γ's, and neutrinos. Consider the case for which the decay electron, coming from the target counter 5, was emitted in the direction of crystal X (see Fig. 1). In order that this electron be counted, we required that it pass through counters 3 and 4, as well as give a pulse in counter 5. Thus an electron in crystal X was detected if it produced a 534 coincidence. In this arrangement the electron solid angle ($0.006\times 4\pi$) was determined by counter 3, which was $\frac{1}{4}$ in. in thickness and 3 in. in diameter. In order to eliminate background from prompt scatters of incoming pions, the beam counter 2 was placed in anticoincidence with electron counters, making the complete electron requirement $534\bar{2}$.

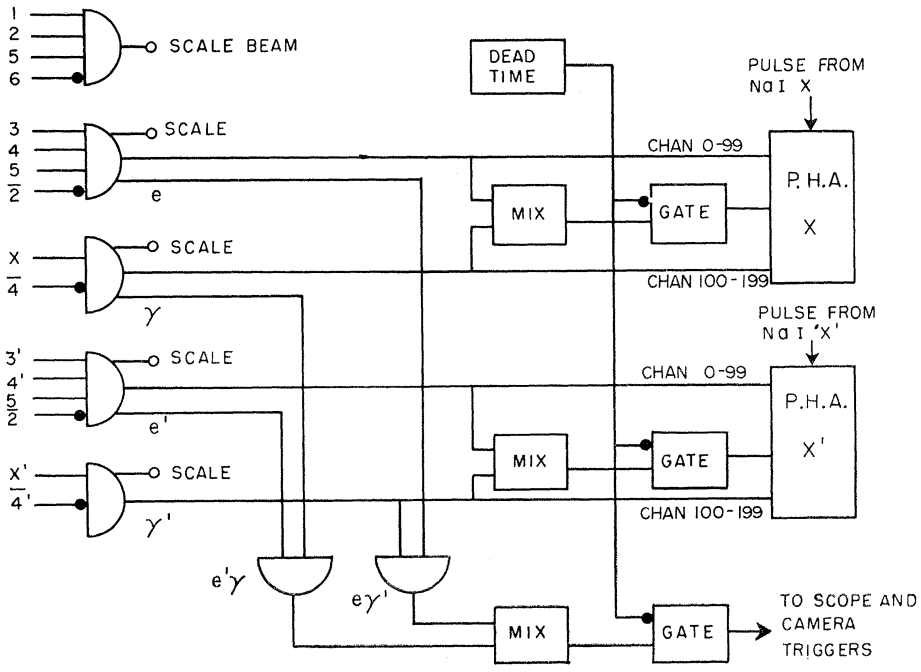

FIG. 2. Diagram of the electronic logic.

It was desired to detect the radiative decay events with angles near 180°. For electrons in crystal X, it was therefore necessary to detect the decay γ entering crystal X'. To do this counter 4′, which covered completely the face of the NaI crystal, served as an anticounter for charged particles entering the crystal. Thus, a γ in X' was signalled by a $\bar{4}'X'$ anticoincidence. The γ solid angle ($0.012\times 4\pi$) was determined by the 3-in.-thick lead collimator between target and crystal, which was needed to minimize edge effects in the NaI crystal. The collimator was designed with conical aperture, having an inner diameter varying from $4\frac{1}{2}$ in. to $5\frac{7}{8}$ in., in order to minimize scattering from the collimator edge and avoid excessive loss of solid angle.

It can be seen that the experimental layout is essentially symmetrical in the primed and unprimed sides. This enabled us to double the counting rate by accepting the opposite type of event: an electron entering crystal X', satisfying the electron coincidence requirement $53'4'\bar{2}$, and the accompanying decay γ interacting in crystal X (with no pulse from counter 4) and so satisfying the γ requirement $\bar{4}X$.

A diagram of the logic for the experiment is shown in Fig. 2. The logic included the coincidence circuits that determined when there was an electron or a γ in crystal X, denoted by e or γ, or an electron or γ in crystal X', denoted by e' or γ'. The pulses from the two NaI crystals were fed into the two corresponding pulse-height analyzers, also labeled X and X'. Either an e or a γ coincidence output pulse served to gate analyzer X on; the pulse height from crystal X was then stored in a 100-channel block in this analyzer, there being one such block for electrons and another for γ's. Comparable 100-channel blocks were used in analyzer X' for the pulses from crystal X', and thus there were stored separately the single-electron spectrum and the single-γ spectrum from each crystal. These gave the background spectra, which were used in the analysis for subtracting accidental background, and for calibrating the relative crystal gain for each 3-h run.

The radiative decay events were determined by taking electron-γ coincidence from opposite sides—$e\gamma'$ for type-1 events and $e'\gamma$ for type-2 events. The coincidence output from either type event activated the mixing gate, which triggered two dual-beam oscilloscopes and a camera-drive circuit. Pictures were taken of the two crystals pulses X and X', the pulses from the electron counters 3 and 3′, and the pulse from the target counter 5. These pictures enabled us to extract, after timing and pulse-height analysis, the observed rate and two-dimensional energy spectrum for electron-γ decay pairs.

Scalers were also used, as shown in Fig. 2, to count the number of stopped pions, the number of single electrons and γ's on each side, and the number of real events of each of the two types, $e\gamma'$ and $e'\gamma$; all of these data were checked continually during the experiment to verify that the counters and logic were operating properly.

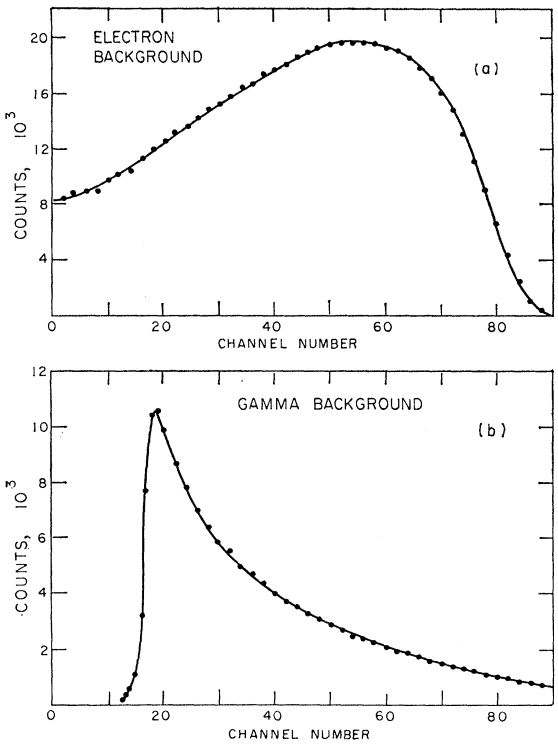

FIG. 3. (a) Example of a single-electron spectrum (electron background) stored in the pulse-height analyzer X. The endpoint of the upper edge of the spectrum is about 53 MeV. (b) Example of a single-γ spectrum (γ background) stored in the pulse-height analyzer X. The low-energy cutoff corresponds to 12 MeV.

There was also included in the system a dead-time output which gated off the scalers and all of the slow logic—the pulse-height analyzers, oscilloscopes, and camera-drive circuit. This dead-time output signal was on for a 1-sec period following each camera trigger to allow for camera advance, and was also activated during the unused part of the cyclotron beam cycle, which was adjusted to avoid using the sharp "burst" of beam that would have augmented the accidental rate.

In the course of the experiment about 2.4×10^{10} pions were stopped. A total of 9561 pictures for the radiative decay were obtained, an average of one picture every 2 min, of which 8674 were ultimately used for all calculations. (The others, for which timing characteristics had not yet been optimized, were used only for the electron-γ energy spectrum.) We also obtained 16 000 pictures of nonradiative decay events to use for calibration of the crystal pulse heights. Finally, there were collected in the pulse-height analyzers, for each 3-h run of radiative decay events, the spectra of the corresponding single-electron and single-γ events in each of the two crystals. Typical examples of such spectra are shown in Fig. 3.

At the end of the experimental run, we scanned the beam distribution over the 4 in.$\times$4 in. area of the target.

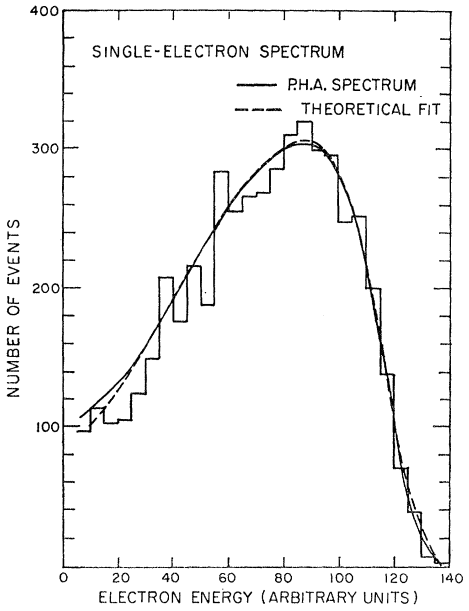

FIG. 4. Histogram of measured single-electron spectrum (from pictures of the nonradiative decay) and the corresponding curves for the theoretical nonradiative decay spectrum and the pulse-height analyzer electron spectrum.

This was done with a $\frac{1}{4}$-in.$\times\frac{1}{4}$-in.$\times\frac{1}{4}$-in. scanning counter (mounted on a precisely calibrated transport), in coincidence with the beam counters, giving the stopping intensity over the target area. These data were combined with information on the stopping distribution along the path of the beam, to give the complete stopping distribution throughout the target.

III. DATA ANALYSIS

Table I lists the 2992 events rejected when scanning criteria were imposed. Events were rejected if the electron counter pulse 3 (or 3′) was above a specified cutoff; if the peak of either crystal pulse X or X' was not visible (a high-energy cosmic-ray event); or if the event lacked a γ crystal pulse and so was an erroneous trigger (there was a lower limit of 12 MeV on the γ energy set by a discriminator). In addition, in order to save measuring time and cut down somewhat on the accidental contribution, we rejected all events which had an extra pulse in the target counter 5 such that the spacing between normal and extra pulses was less than 100 nsec. This was done since most accidental events consisted of an electron passing through one electron telescope in time coincidence with a bremsstrahlung γ radiated by a different electron entering the opposite crystal. Pictures of accidentals thus usually showed two target counter pulses, unless their spacing was less than the resolution for such pulses. Therefore, we rejected events with two target counters pulses within 100 nsec, a time interval somewhat less than the time gate set electrically by the electron-γ coincidence circuit. To allow for this rejection criterion, a correction term was included in obtaining the observed radiative decay rate. A similar correction term was needed for a final group of rejected events, the 296 pictures which were unmeasurable due to overexposure, underexposure, missing traces, etc.

TABLE I. List of events rejected in scanning.

Criterion	Number of pictures rejected
Pulse in counter 3 (or 3′) above cutoff	478
Peak not visible in X or X'	491
Gamma crystal pulse missing	29
Extra pulse in counter 5 within 100 nsec	1698
Unmeasurable event	296
Total number rejected	2992
Number remaining	5682

For all pictures which survived the rejection criteria, we measured (a) the amplitudes of the NaI crystal pulses, X and X', and of the pulse from the target counter 5; and (b) the timing of the electron counter pulse 3 (or 3′), the γ crystal pulse X' (or X), and the target counter pulse 5. The zero time was chosen to be the start of the electron counter trace 3 (or 3′); the timings of both 3 and X' (or of 3′ and X) were taken with respect to this zero. Thus any error in the zero cancelled when the relative electron-γ timing was calculated. Then use of the relative timing distribution, for events within appropriate energy cutoffs, enabled us to minimize the contribution of accidentals by taking the smallest possible time gate for real events.

We also measured, for calibration purposes, the electron crystal pulse heights for the 16 000 pictures taken of nonradiative decay events. The spectrum from these events (Fig. 4) was fitted to the expected nonradiative electron spectrum, in which was included the effects of folding in the energy loss resolution and the NaI resolution function. The best fit obtained ($\chi^2=8.3$ for 11 channels) gave directly the absolute pulse-height calibration for the NaI crystals, for both γ's and electrons.

It was in practice necessary to calibrate the crystal amplitudes separately for each 3-h run, since the gain of the phototubes viewing the crystal drifted with time. The nonradiative decay spectrum for each such run had been stored (for both crystals) in the pulse-height analyzers, and could therefore be used for this relative calibration. The nonradiative decay spectrum from the pulse-height analyzers was also used for a fit to the expected nonradiative spectrum (again including the effects of energy loss and crystal resolution functions). Several sets of analyzer spectra were combined to give $\sim 10^7$ events, and the fit so obtained was used to determine the precise magnitude of the energy loss in the counters, and the exact height of the low-energy tail of the resolution function, which depended on the collimation before the crystal. An excellent fit (Fig. 4)

was obtained by optimizing just these two parameters, which were then used in the calculations for the radiative decay spectrum.

A calibration was also made of the pulses from the target counter 5, in order to reduce the error due to the spread in energies from electrons originating at all possible points in the 1-in.-thick target. For the radiative decay events, then, the measured electron energy x was taken to be the sum of the energy loss in the NaI crystal (from the crystal pulse height) and the estimated energy loss in the target counter. Both x and y (the measured energy of the γ) were expressed in units of the maximum energy 52.8 MeV, so that the maximum energies became $x=1.0$ and $y=1.0$.

Cutoffs were then chosen for the upper and lower ends of the energy spectrum. The upper cutoff, chosen to eliminate high-energy cosmic-ray background, was 1.25 for both x and y. (A value larger than 1.0 was required because of the high-energy tail of the crystal resolution function.) The 190 events with energies above these cutoffs yielded spectra in good agreement with the background spectra for that energy range.

For low-energy γ's, an electronic cutoff had been set during the experiment. However, the discriminator setting determining this cutoff drifted with time and had to be readjusted several times during the course of the experiment. A low-energy γ cutoff of $y=0.275$ was therefore chosen in the analysis, a value above the highest setting of the discriminator cutoff. For the low-energy electrons, in contrast, there was no electronic cutoff; the only requirement for electrons was a 534 (or 53′4′) coincidence, which could be satisfied by an electron stopping in counter 4 before reaching the crystal. For those events with a zero or very small electron energy, it was verified that the γ spectrum, after subtraction of background, was consistent with the spectrum expected from electrons stopping in counter 4. However, the background was too large ($\sim$80%) to permit any information to be extracted from these events. Therefore, a lower cutoff was set on the electron energy of $x=0.15$, and it was also required that the electron give a measurable pulse in the NaI crystal. These requirements were allowed for in the calculation of the expected spectrum and rate, as discussed below. It was also determined, as a useful check, that the final result obtained for the parameter η was not at all sensitive to the choice of electron energy cutoff.

An upper cutoff was also set on the heights of pulses from the target counter. Some measured events had target counter pulses well beyond the maximum expected for an electron of that energy range, even in traversing the full width of the target. These events may have been due to scattered pions, for example, with an anti-inefficiency of the beam counter 2. An upper limit was therefore set for the counter 5 pulse, and 70% of the events rejected because of this limit were accidentals.

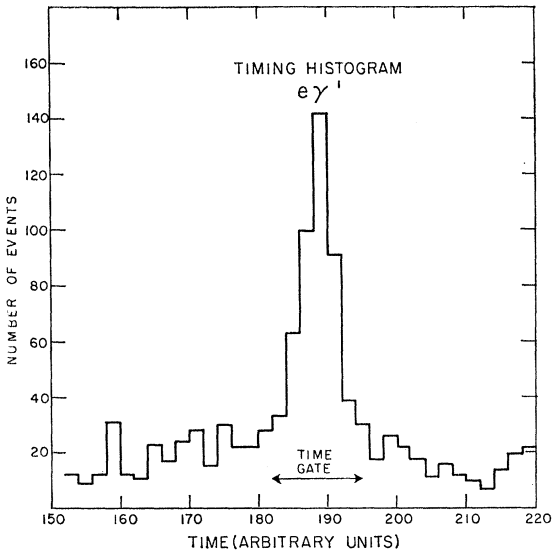

FIG. 5. Timing histogram for $e\gamma'$ (type-1) events within the energy cutoffs and surviving all scanning and measuring criteria. The time gate chosen corresponds to 20 nsec.

One additional criterion was included for rejection of events. The γ's, it is noted, were distinguished from charged particles by the requirement of an anticoincidence of counter 4 (for crystal X) or counter 4′ (for crystal X'). We expected, though, at least 1% inefficiency in these anticoincidences, based on counting rates taken during the experimental run. This anti-inefficiency generated about 200 spurious events which had two electrons, instead of one electron and one γ, entering the crystals. This was allowed for by rejecting all measured events having electron pulses in both counters 3 and 3′ (within their normal timing range).

After applying all the cutoffs and rejection criteria described, we were left with 3276 events. From the relative electron-γ timing for these events, timing histograms were prepared for both $e\gamma'$ (Fig. 5) and $e'\gamma$ events. From these histograms, which contained only events within the cutoffs, an optimum timing gate of 20-nsec width was chosen. The events within the time gate were designated as reals; those outside the gate, as accidentals. In order to obtain the amount of background within the time gate, a determination was made of the number of accidentals within 16 nsec of either edge of the gate. The resulting number, 610, corresponded to a background within the gate of 379 events, with an error $\sigma_{\text{back}}=(379/610)\times(610)^{1/2}=15.3$. Thus the total background in the experiment was 379 ± 15 events.

It should be noted that the apparent decrease in rate away from the time gate was due to the scanning criterion of rejecting the events with an extra pulse (within 100 nsec) in counter 5. Near the time gate, this extra pulse was often not resolved because of its proximity to the first counter 5 pulse, so that the event would be measured rather than rejected in scanning.

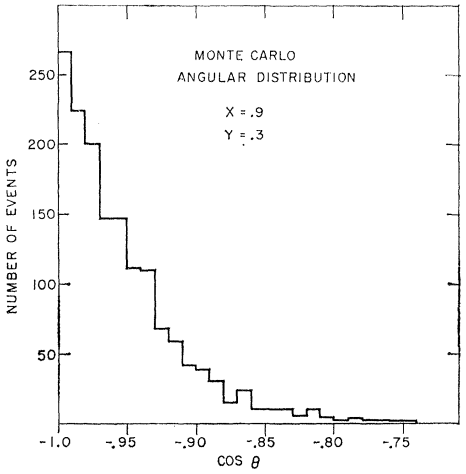

FIG. 6. A typical angular distribution obtained from the Monte Carlo calculation. The initial particle energies for the distribution are $x=0.9$ and $y=0.3$.

If the timing distribution had been taken with this criterion removed, then the distribution would have become essentially flat outside the time gate.

With the time gate chosen, it was now possible to classify all the measured events. The results are shown in Table II. The 1173 real events included the background of 379 events (32%) within the time gate, and so gave 794 radiative decays. This experimental number was augmented by two corrections: An adjustment was needed, first of all, for the 1698 events rejected because of an extra pulse in counter 5 within 100 nsec of the original pulse in that counter. To obtain this correction, we measured the electron-γ timings, but not the amplitudes, of 60% of the rejected events, obtaining 70 events with real timing. Since 32.7% of all real events fell within the energy cutoffs, this contributed a correction of 38±4. A second correction was for the 296 unmeasurable events; this number was multiplied by the fraction of all scanned events which did consist of real events within the cutoffs. There resulted a contribution of 30 events.

The errors (including that of background subtraction) were then added in quadrature, and there resulted finally for the experimental number of radiative decay events,

$$N_{\text{expt}}=862\pm39.$$

TABLE II. Classification of measured events.

Type of event	Number of events
Reals	1173
Accidentals	2103
$x>0.15$ and no electron crystal pulse	107
$x<0.15$	399
$x<0.15$ and no electron crystal pulse	563
$y<0.275$	750
$x<0.15$ and $y<0.275$	156
$x>1.25$, $y>1.25$, or x and $y>1.25$	190
Counter 5 pulse>40 units	45
Both 3 and 3′ pulses	196
Total	5682

IV. THEORETICAL PREDICTIONS

The theoretical expression for radiative muon decay was derived by Fronsdal and Überall[9] as an explicit function of the muon decay coupling constants. With the assumption that $\rho=\frac{3}{4}$, and neglect of the asymmetry term (since the muons in the present experiment are unpolarized), the transition probability can be written as

$$dN_\gamma=\frac{e^2m_\mu{}^5}{3\times2^{16}\pi^6}dxdyd\Omega_e d\Omega_\gamma \times\omega[A_r(x,y,\Delta)+\eta B_r(x,y,\Delta)], \quad (1)$$

where

$$x=\frac{E_e}{\frac{1}{2}m_\mu},\quad y=\frac{E_\gamma}{\frac{1}{2}m_\mu},\quad \Delta=1-\cos\theta,$$

$\theta=$ electron-γ angular correlation,

and

$$\omega=4a+4b,$$

$$\eta=\frac{1}{2}\frac{(a/b)}{1+(a/b)},$$

with

$$a=|g_S|^2+|g_S'|^2+|g_P|^2+|g_P'|^2,$$
$$b=|g_V|^2+|g_V'|^2+|g_A|^2+|g_A'|^2,$$

in the usual notation for the muon-decay coupling constants, The functions $A_r(x,y,\Delta)$ and $B_r(x,y,\Delta)$ are given explicitly in the Appendix. The transition probability is thus a function of one parameter in particular, η, which is unique to the radiative decay and which measures directly the fraction of S-T-P entering into muon decay. In the case that $\xi=-1$ for muon decay,[11] it can be shown that η is related to the electron polarization P by the expressions

$$P=1-4\eta \quad \text{(positrons)}.$$

In this experiment, the electron-γ correlation angle θ was not measured. It was therefore necessary to average the term $(A_r+\eta B_r)$ over the angular distribution, which depended on the geometrical configuration and on the beam-stopping distribution. The angular distribution was obtained by carrying out a Monte Carlo calculation run on the Columbia University IBM 7094 computer. The Monte Carlo program included many small effects which were of significance for the angular distribution: The electron was subject to multiple scattering, bremsstrahlung, and ionization energy loss straggling; and the γ could undergo Compton scattering, for example, at the edge of the lead collimator. All of these

[11] M. Bardon, D. Berley, and L. M. Lederman, Phys. Rev. Letters **2**, 56 (1959); R. Plano, Phys. Rev. **119**, 1400 (1960).

effects depended on the energy of the particle, and hence the Monte Carlo calculation was run separately for a large number of distinct electron and γ energy combinations, covering the whole range of energies for both particles. A typical angular distribution from the Monte Carlo calculation is shown in Fig. 6.

The functions $A_r(x,y,\Delta)$ and $B_r(x,y,\Delta)$ were averaged over the particular angular distribution obtained for the energies (x,y). The averaging was done for only those angles above a kinematic cutoff: Conservation of energy and momentum forbids angles below a minimum angle $\Delta_{\min}=2(x+y-1)/xy$. This cutoff changes not only the average values of A_r and B_r, but also the effective solid angle for the decay, making the solid angle a function of x and y. Now the Monte Carlo calculation generated the angular distribution for all electron-γ events that were geometrically possible, regardless of kinematics. The procedure used was, first, to average A_r and B_r over those angles above the cutoff; then to multiply by the ratio of the number of kinematically possible events $(\Delta\geq\Delta_{\min})$ to the total number of generated events. The resulting functions, denoted by $A(x,y)$ and $B(x,y)$, thus included implicitly the dependence of solid angles on energies.

It was necessary to include in the calculations the requirements for acceptance of electrons set in the analysis, namely, that the electrons produced a 534 coincidence in the electron telescope and also gave rise to a measurable pulse in the NaI crystal. Moreover, the expression $(A+\eta B)$ gives the *total* number of electron-γ pairs emitted with energies x and y, and so must be corrected for electrons stopping in the target or lost through multiple scattering. This correction was made by multiplying A and B by an electron efficiency function $\epsilon(x)$, which was defined to be the fraction of electrons that did satisfy the requirements. The efficiency function was taken directly from the Monte Carlo calculation mentioned above, and so included, for example, the effect of high-energy electrons lost due to the emission of an energetic bremsstrahlung γ, so that the electron stopped before reaching the crystal. A smooth fit was made to the calculated points of the efficiency function (Fig. 7).

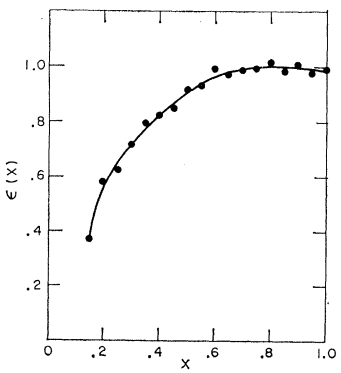

FIG. 7. Electron efficiency function $\epsilon(x)$, the relative number of electrons satisfying the electron requirements (e.g., not stopping in counters 5, 3, or 4) for initial electron energy x. The curve is a least-squares fit through the experimental points calculated by the Monte Carlo program.

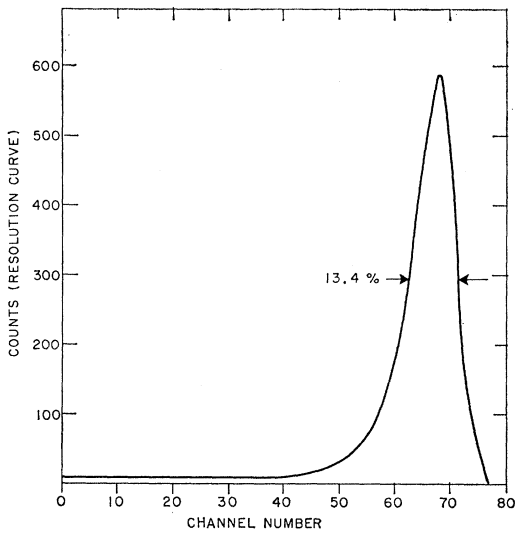

FIG. 8. Resolution function for the NaI crystals (Ref. 12).

The calculations of $A(x,y)$ and $B(x,y)$ were carried out separately for the two types of events, since the experimental layout was not exactly symmetrical in the sides X and X'. The resulting functions, for each type of event, were averaged together with a weight proportional to the product of electron and γ solid angles. It was then necessary to fold in the resolution functions of the NaI crystals. The folding was done simultaneously for x and y, and could be expressed by the following equation (A' denotes the function after folding):

$$A'(x,y)=\int\int A\left(\frac{x}{q_1},\frac{y}{q_2}\right)R(q_1)R(q_2)dq_1dq_2,$$

and similarly for B'. In this expression, q_1 and q_2 are the variables for the electron and γ resolution function, respectively. The same function $R(q)$, shown in Fig. 8, was used for both electrons and γ's, since it is known that high-energy particles of the two kinds produce comparable showers in sufficiently large crystals. The shape and width of $R(q)$ was assumed to be known from a previous experiment,[12] and the exact height of the low-energy tail was taken from the best fit to the nonradiative decay spectrum (see above).

The expected number of radiative decays is proportional to the term $[A'(x,y)+\eta B'(x,y)]$. In order to compare the observed and expected rates, and thus obtain a best value for the parameter η, we normalized the radiative decay rates to the corresponding rates for the nonradiative decay. Specifically, the normalization was to the number of electrons observed in the high-energy region of the nonradiative spectrum, from $x=0.35$ to $x=1.0$. This procedure made it unnecessary for us to determine the electron solid angle or the

[12] L. G. Pondrom and A. Strelzoff, Rev. Sci. Instr. **34**, 362 (1963).

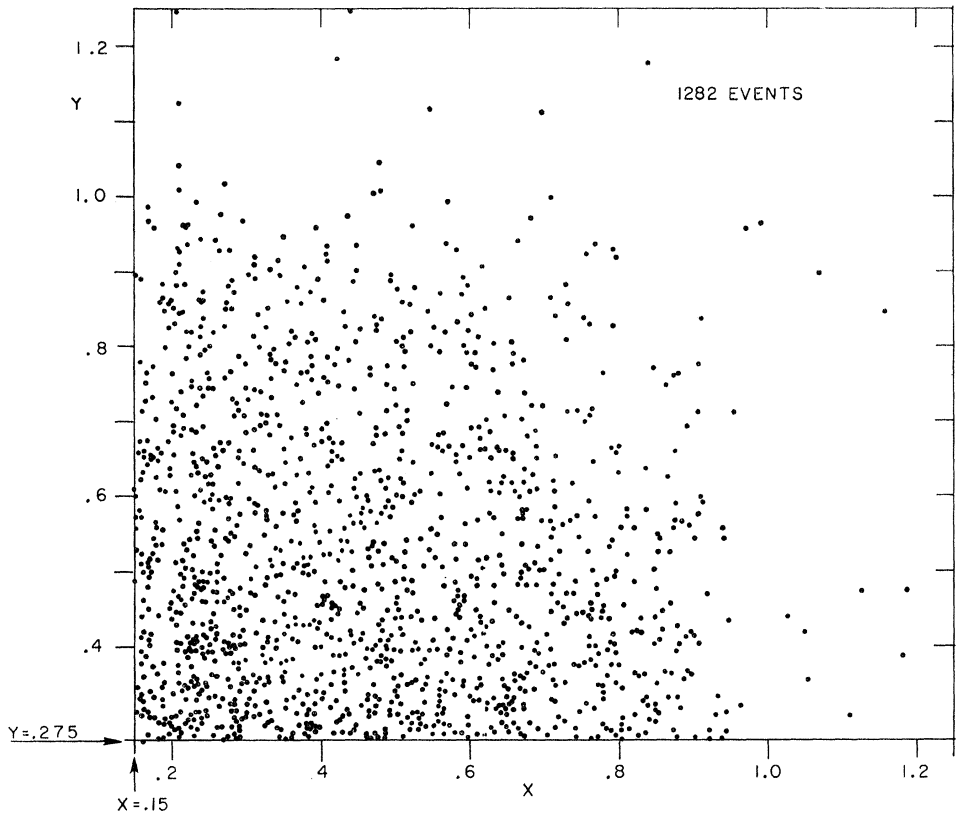

FIG. 9. Scatter plot of the (x,y) pairs used for the maximum-likelihood calculation of η. The events include 32% background.

efficiencies of the beam counters. The use of the high-energy region of the electron spectrum, as collected in the pulse-height analyzers, also eliminated the low-energy background (such as scattered pions with an anti-inefficiency of counter 2).

The transition probability for the nonradiative mode, assuming as before $\rho=\frac{3}{4}$ and unpolarized muons, is[9]

$$dN_e=\frac{m_\mu{}^5}{3\times 2^{10}\pi^4}\omega dx d\Omega_e\, x^2(x-\tfrac{3}{2}),$$

where x and ω are as above. The factor $x^2(x-\frac{3}{2})$ is denoted by $F(x)$. We folded numerically into $F(x)$ the following: (a) the distribution of energy losses in target and electron counters, and (b) the resolution function of the NaI crystals. The resulting folded spectrum, which we denote by $F'(x)$, gave a good fit with the electron spectrum from the pulse-height analyzers, as observed in Sec. III.

The expected number of radiative decays, based on normalization to the nonradiative mode, can now be written as

$$N_{\rm rad}=N_{\rm nonrad}\left[\frac{e^2 d\Omega_\gamma}{2^4\pi^2}\right]\int_{0.15}^{1.25}dx\int_{0.275}^{1.25}dy\,(A'+\eta B')\Big/\int_{0.35}^{1.25}dx\,F'(x)$$

where the integrals are taken between limits corresponding to those for the observed events. The various factors are evaluated as follows:

$$\int\int(A'+\eta B')dxdy=4.51-1.45\eta,$$

$$N_{\rm nonrad}=8.087\times 10^7(\text{type } e)+7.839\times 10^7(\text{type } e'),$$

$$\int F'dx=0.1744(\text{type } e)+0.1704(\text{type } e'),$$

and $\Delta\Omega_\gamma=0.0116\times 4\pi$ (from a Monte Carlo calculation). There results

$$N_{\rm rad}=872-282\eta.$$

The number of nonradiative decay events was taken from the pulse-height analyzer spectra. It was therefore necessary to add a 2.3% correction for the dead time of the analyzers, since there was no electronic gate to prevent the oscilloscopes and cameras from triggering during this dead time. No dead-time correction is needed for the radiative decays, however, since after each camera trigger there was a 1-sec dead-time pulse applied to all the logic, including the analyzers (Fig. 2).

The final expression for the expected number of radiative decay events, including dead-time correction, is then

$$N_{\rm rad}=898-288\eta.$$

V. RESULTS AND DISCUSSION

The data in the experiment consisted of electron and γ energies for each event, giving a two-dimensional energy spectrum for the decay. A scatter plot of this electron-γ spectrum is shown in Fig. 9. For maximum sensitivity to coupling constants, as determined from the parameter η, this complete two-dimensional spectrum was needed. However, for purposes of examining the over-all agreement with experiment, given that the total number of events was not large, it was more effective to look at the integrated spectrum, the number of events as separate functions of electron and γ energies.

Figure 10 shows the experimental and theoretical energy spectra for the electrons. It is noted that the two theoretical curves give the absolute rate for the indicated value of η. Comparing the experimental histogram to the curve for $\eta=0$ (pure $V-A$), we obtained $\chi^2=7.6$ for 14 degrees of freedom, corresponding to 90% confidence level. For the $\eta=0.5$ curve (pure $S-T$) in contrast, there was obtained $\chi^2=19.8$ for 14 degrees of freedom, which is equivalent to a confidence level of 14%.

The experimental and theoretical energy spectra for the gammas are given in Fig. 11. Again, the theoretical spectra give the expected rate for that value of η. The comparison of spectra produced $\chi^2=15.3$ for 14 degrees of freedom, for the $\eta=0$ curve, which corresponds to 43% confidence level; and $\chi^2=31.9$ for 14 degrees of freedom for $\eta=0.5$, or a confidence level of 0.005%. It is clear that for both γ and electron spectra, good agreement with the radiative decay theory has been obtained for the case $\eta=0$ (pure $V-A$ coupling).

A maximum-likelihood calculation was performed to extract the best value of η from the two-dimensional energy spectrum. The logarithmic derivative of the normalized likelihood function, $\partial(\ln\mathfrak{L})/\partial\eta$, which is set equal to zero to give the best value of η, was

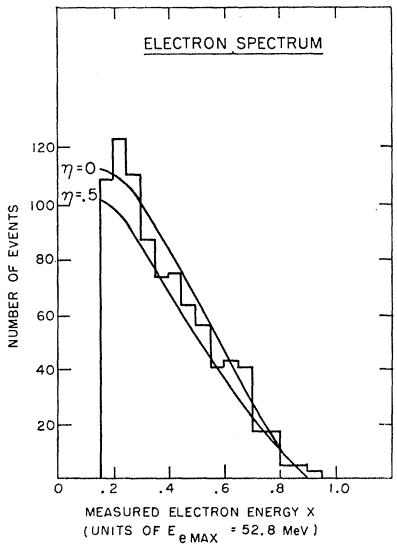

FIG. 10. Electron spectrum for the radiative decay. The theoretical curves are for $\eta=0$ and $\eta=0.5$.

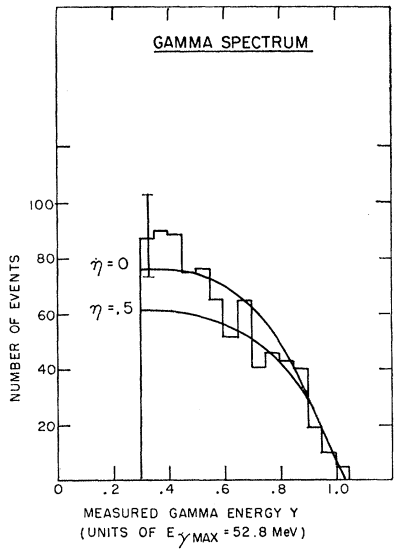

FIG. 11. Gamma spectrum for the radiative decay. The theoretical curves are for $\eta=0$ and $\eta=0.5$.

given by

$$S(\eta)\equiv\frac{\partial\ln\mathfrak{L}}{\partial\eta}=\sum_K\frac{B'(x,y)}{A'(x,y)+\eta B'(x,y)}-N\int\int B'dxdy\Big/\int\int(A'+\eta B')dxdy,$$

where N is the number of observed events, and the sum is taken over all observed energy pairs (x_k,y_k). To avoid having to group the data into energy cells, with resulting loss of precision, we included the background not by subtraction from the experimental spectrum but rather by addition to the theoretical distribution $(A'+\eta B')$. It was assumed that the electron background and the γ background were two independent distributions, and hence the complete background distribution could be expressed as the product of the two, $Z(x,y)=Z_e(x)\times Z_\gamma(y)$, with Z_e and Z_γ the electron and γ spectra obtained with negligible statistical error in the pulse-height analyzers. Thus the substitution was made $A'(x,y)\rightarrow A'(x,y)+Z(x,y)$, with Z normalized to give the correct accidental contribution (32%). The calculation of $S(\eta)$ was done with 1282 events; the maximum-likelihood result obtained is

$$\eta=-0.045\pm0.27 \text{ from the spectrum,}$$

where the error is purely the statistical one, obtained as the inverse square root of the expectation value of $\partial S/\partial\eta$.

An independent and more accurate value of the parameter η is obtained by comparison of the observed rate with the rate expected (for the given energy cutoffs) as a function of η. There results the equality

$$862\pm39=898-288\eta,$$

giving

$$\eta=0.12\pm0.13 \text{ from the total rate.}$$

TABLE III. Estimates of systematic errors.

Source of error	Assumed error
Energy calibrations for x and y	0.03
Normalization to electron rate	0.03
Monte Carlo calculation of A and B	0.03
Background subtraction	0.02
Energy loss	0.02
Crystal resolution function	0.02
Gamma solid angle	0.01
Total (added in quadrature)	0.06

The separate results of the calculation of η from the spectrum and from the rate were combined statistically, and give $\eta=0.09\pm0.12$. An estimate was made of the systematic error in the experiment for each of the possible sources of such error. These systematic errors were taken to apply to the combined result for η, since the individual systematic errors for spectrum and rate, unlike the corresponding statistical errors, are not independent quantities. Table III gives the estimated standard error in the various cases. The energy calibrations, electron rate normalizations, energy loss, and crystal resolution function were all determined (at least in part) by a χ^2 fit, and so the error in each case was obtained by observing the change in η corresponding to a change of one standard deviation in the value of η. The total systematic error is 0.06, and is combined in quadrature with the statistical error to give a total error of 0.14.

The final result for η, the parameter unique to the radiative decay, is thus

$$\eta=0.09\pm0.14,$$

in agreement with $V-A$ theory for muon decay. It is noted that with the assumption $\xi=-1$ for muon decay, the relation $P=1-4\eta$ may be used to obtain the electron polarization as $P=+0.65\pm0.56$, again consistent with the observed value of $P=+1.0$ (for positrons).

ACKNOWLEDGMENTS

We would like to thank the entire staff of the Columbia Nevis Cyclotron Laboratories, and in particular the scanning technicians, Al Kenny and Ken Stewart, for making this experiment possible. We are also grateful to Professor Samuel Devons and Professor Leon Lederman for helpful discussions concerning the experiment. One of us (E.DiC.) would like to thank Columbia University for the hospitality of the Nevis Laboratories.

APPENDIX: EXPLICIT FORMULAS FOR THEORETICAL DISTRIBUTION

The following are the complete expressions for the theoretical functions $A_r(x,y,\Delta)$ and $B_r(x,y,\Delta)$ of Eq. (1) based on Eqs. (4a) and (4b) of Fronsdal and Überall[9] with the associated formulas in their Appendix:

$$\begin{aligned}A_r(x,y,\Delta)=\frac{1}{y}\Big\{&\Big[\Delta+\frac{2}{\mu^2x^2}\Big]^{-1}8[y^2(3-2y)+6xy(1-y)\\&+2x^2(3-4y)-4x^3]+8[-xy(3-y-y^2)\\&-x^2(3-y-4y^2)+2x^3(1+2y)]\\&+\Delta\times2[x^2y(6-5y-2y^2)-2x^3y(4+3y)]\\&+\Delta^2\times2x^3y^2(2+y)\Big\},\end{aligned}$$

$$B_r(x,y,\Delta)=\frac{1}{y}[16xy^2(-1+y+2x)-\Delta\times8x^2y^2(1+y)].$$